J. Iron Steel Res. Int. (2020) 27:282–294
https://doi.org/10.1007/s42243-020-00363-7

ORIGINAL PAPER

Reaction kinetics during direct alloying of manganese ore cored wire

Wei Wu[1] · Qi Gao[1] · Bo Zhang[1] · Hua-dong Meng[1] · Lu Lin[1,2] · Jia-qing Zeng[1]

Received: 9 November 2018 / Revised: 10 April 2019 / Accepted: 10 April 2019 / Published online: 27 February 2020

Abstract
In order to increase the reaction rates between the molten steel and the slag and cut down the reduction time when the top slag of manganese ore is added into the molten steel, a method of directly alloying manganese ore has been experimented in a 500-kg induction furnace. The results show that the manganese yield is greater than 90% when the wire feeding method is used. The manganese yield is 43.26% within 1 min. In contrast, the manganese yield for the top-slag adding process is only 10.98% for the same duration. The mass transfer rate of the manganese is greater in the molten steel than in the slag, and the limiting factor is the mass transfer rate of the manganese in the slag in the period of 10−30 min. The slag composition area is closer to the area of high melting point for the wire feeding method than for the top-slag adding process. During the slagging process, refining slag composed of CaO and SiO_2 is formed after 15 min; after 25−30 min, refining slag with a high basicity is formed and consists of CaO, SiO_2 and Al_2O_3.

Keywords Manganese ore · Cored wire · Direct alloying process · Reaction kinetics · Mass transfer rate

1 Introduction

Direct alloying of manganese ore [1–6] in the steelmaking process, which may shorten the process, reduce pollution and reduce production costs, has promising prospect. Shimoo et al. [7, 8] studied the reduction rate of MnO in $CaO–Al_2O_3–MnO$ and silicate slags by using a graphite crucible and determined that the reaction rate is controlled by the chemical reaction process at the slag–graphite interface. However, when carbon is added to the slag, a first-order reaction occurred. Xu et al. [9] investigated the reduction kinetics of MnO within carbon-saturated liquid iron and found that the apparent reaction is in the second order when no carbon is added to the slag. Ashizuka et al. [10] studied the rate of MnO reduction from slag by carbon-saturated iron at 1500–1600 °C and determined the rate-limiting step of MnO reduction by the electrochemical method. Kim and Jung [11] studied the manganese distribution of $CaO–SiO_2–FeO–MnO$ slag in equilibrium with solid Fe. It is observed that the manganese distribution ratio decreased with increasing CaF_2, which is believed to have the effect that it would increase the activities of MnO and FeO. Shinozaki et al. [12] studied the reduction behavior of carbon-containing MnO slag in liquid iron at 1600 °C. It is believed that the rate of MnO reduction reaction is restricted by the mass transfer of the reaction component. According to the literatures [13–15], for the carbon reduction of manganese ore in different atmospheres, the optimal C/O value in the agglomerate is 1.2, and excess reducing agent has no obvious effect on the improvement in the agglomeration degree. The smaller the amount of slag, the higher the manganese yield [16]. Adding calcium oxide or magnesium oxide to manganese ore helps to reduce the content of manganese

✉ Qi Gao
gaoqi_61617664@126.com

Wei Wu
wuweineu@163.com

Bo Zhang
zhangbo530925@163.com

Hua-dong Meng
menghuadong@126.com

Lu Lin
linlu_luke@sina.com

Jia-qing Zeng
zengjiaqing@vip.sina.com

[1] Metallurgical Technology Research Department, Central Iron and Steel Research Institute, Beijing 100081, China

[2] State Key Laboratory of Refractory and Metallurgy, Wuhan University of Science and Technology, Wuhan 430081, Hubei, China

oxide in slag [17]. Suitable thermodynamic and kinetic conditions are the key to efficient reduction of manganese ore [18].

However, in the aforementioned studies, for the direct alloying process, usually the manganese ore was added to the molten steel from the top-slag adding, in which the reduction of the manganese ore only occurs in the liquid–liquid interface between the slag and molten steel, and the effect is always not ideal [19, 20]. In the tapping process of the converter, the manganese yield is about 80% [21–23]. Therefore, it is necessary to develop a method to increase the contact area between the manganese ore and the molten steel to improve the efficiency of the manganese reduction reaction.

In order to create better metallurgical kinetic conditions to increase the reaction rate of manganese ore direct alloying and the manganese recovery, this paper extends the method that a cored wire is fed directly into the molten steel bath, and the material in the cored wire comes in direct contact with the molten steel. The reaction area is increased, which helps to increase the reaction rate of the manganese ore reduction. Therefore, in this study, a manganese ore direct alloying technology was tested, and the efficiency of direct alloying, the kinetics and the slag phase equilibrium of manganese ore cored wire were also discussed.

2 Materials and methods

2.1 Experimental materials and preparation

A ϕ8-mm manganese ore cored wire is made from a 0.2-mm-thick 08Al steel, a thin strip of steel and a mixture of manganese ore powder, lime powder and anthracite powder using a cored wire machine. The net mass of the mixed powder in the finished manganese ore cored wire is 1.2 g/cm. The manganese ore cored wire is composed of manganese ore, lime and anthracite. After dried, crushed and ground, the three types of raw materials are pressed to spheres or fabricated to cored wires by high pressure. The particle size of the raw material is smaller than 0.074 mm, and the drying time is 24 h at 200 °C. The mixing powder ratio and ingredients in the cored wire are shown in Table 1. Manganese ore cored wire finished is shown in Fig. 1.

Table 1 Main raw material composition and content of manganese ore cored wire

Material	Ratio/%	Main ingredients and content
Manganese ore	64	TFe 11.6 wt.%, TMn 42.8 wt.%, SiO_2 16.0 wt.%, P 0.13 wt.%, S 0.016 wt.%
Lime	24	CaO ≥ 95 wt.%
Anthracite	12	Ash 14.98 wt.%, fixed carbon 76.61 wt.%, volatile matter 14.98 wt.%, S 1.63 wt.%

The metal is prepared by industrial pure iron and electrolytic manganese as the main raw materials, that is, [C] < 0.1 wt.%, [Si] < 0.1 wt.% and [Mn] 0.8–1.2 wt.%. The slagging material mainly consisted of lime and lightly burned dolomite. The main deoxidizers are carbon powder, aluminum and ferrosilicon powder.

2.2 Experimental equipment and methods

The experimental equipment and schematic drawing of the 500-kg intermediate-frequency induction furnace and wire feeding machine are shown in Fig. 1. The lining of the medium-frequency induction furnace is knotted with magnesia. The bottom is equipped with a bottom-blowing lance, through which the nitrogen gas is supplied with an intensity of 0.04–0.20 m^3/(t min). The feeding machine is a WX-5BF double-current feeding machine with a feeding speed range of 0.5–4.0 m/s.

First, pure iron and electrolytic manganese were added to prepare the required metal composition. The furnace charge was 200 kg, and the average depth of the molten bath was 300 mm. Second, the heating power of the induction furnace was kept stable when the composition and temperature measured satisfied the planned standard, and the intensity of the bottom-blowing nitrogen was adjusted to an appropriate value. Third, the wire feeding machine was turned on and the wire was fed into the molten steel. After feeding the wire, sampling and temperature measurements were taken. Subsequently, the slag former was added to the molten steel surface. Five minutes later, the deoxidizer was added to the slag surface. The steel and slag samples were obtained every 5 min. The experiment from the wire feeding to the testing end lasted for 30 min.

Six experiments were carried out according to experimental parameters. In order to reduce errors, the wire feeding experiments were repeated twice. In the first and second experiments, the material was fed into the cored wire at a wire feeding speed of 1 m/s and a mixture of aluminum and ferrosilicon powder was used for the deoxidation. In the third and fourth experiments, the wire feeding speed was 1 m/s and ferrosilicon powder was used for deoxidation. In the fifth experiment, manganese ore was added from the top of the furnace, and ferrosilicon powder was used for the deoxidization. In the sixth experiment, manganese ore powder was added from the top of the furnace and a mixture of aluminum and ferrosilicon powder was used for deoxidation. The nitrogen supply intensity at the bottom of the induction

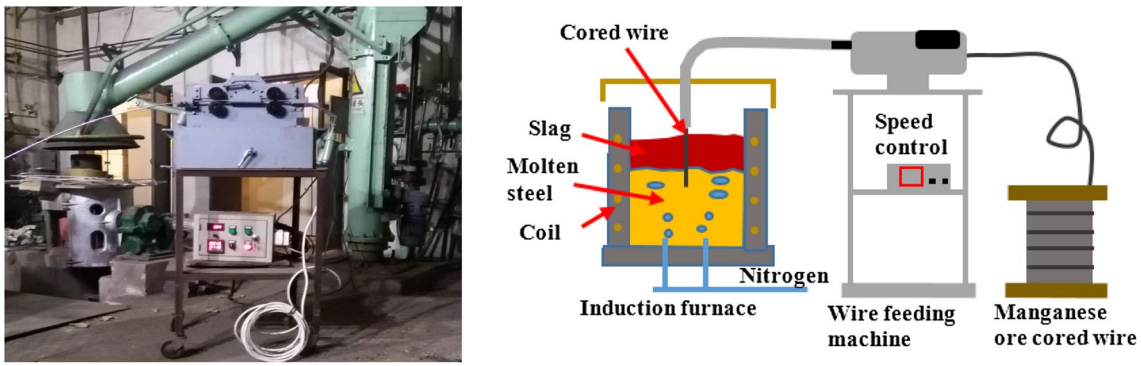

Fig. 1 Experimental equipment and schematic diagram

furnace was 0.08 m^3/(t min), and the experimental temperature was in the range of 1540–1600 °C.

In the experiments, samples of steel and slag were obtained at different time. The steel samples were analyzed by inductively coupled plasma (ICP) spectroscopy, and the slag samples were analyzed by X-ray fluorescence. The temperature was measured using a thermocouple, and the lithofacies of the slag were observed with a scanning electron microscope.

The calculation of the manganese yield is as follows:

$$\eta_{\mathrm{Mn}} = \frac{M \times \left(w_{[\mathrm{Mn}],\mathrm{f}} - w_{[\mathrm{Mn}],\mathrm{i}}\right)}{m \times \alpha} \times 100 \quad (1)$$

where η_{Mn} is the manganese yield; M is the mass of the molten steel; m is the mass of the manganese ore; α is the TMn content of the manganese ore; $w_{[\mathrm{Mn}],\mathrm{i}}$ is the initial manganese content of the molten steel; and $w_{[\mathrm{Mn}],\mathrm{f}}$ is the manganese content in the molten steel at the end of the smelting process.

The manganese distribution ratio between slag and steel is calculated as follows:

$$L_{\mathrm{Mn}} = \frac{w_{(\mathrm{MnO})}}{w_{[\mathrm{Mn}]}} \quad (2)$$

where L_{Mn} is the manganese distribution ratio between slag and steel; $w_{(\mathrm{MnO})}$ is the manganese oxide content of the slag; and $w_{[\mathrm{Mn}]}$ is the manganese content of the molten steel.

3 Experimental results

The experimental results of the six tests are summarized in Tables 2 and 3.

The manganese yield at different time and the manganese distribution ratio between slag and steel calculated by Eqs. (1) and (2) are shown in Fig. 2. Tables 1 and 2 shows that the manganese yield within 10 min is higher for the wire feeding process than for the top-slag adding process. In particular, within 1 min, the manganese yield of the wire feeding process is 43.26% with a range of 30.48%–58.58%. For the top-slag adding process, the average manganese yield is 10.98% with a range of 6.07%–15.90%. The manganese yield is quite similar for the two processes after 30 min. The manganese distribution ratio between slag and steel is lower for the wire feeding process than for the top-slag adding process in the range of 0–10 min. For the range of 10–30 min, the manganese distribution ratio between slag and steel is similar for the two processes.

4 Discussion

4.1 Influencing factors on manganese yield

The decomposition reactions of the manganese oxides in the test are as follows:

$$\mathrm{MnO(s)} = \mathrm{Mn(s)} + \frac{1}{2}\mathrm{O_2(g)} \quad \Delta G^0 = 388,860 - 76.42T \quad (3)$$

$$\mathrm{Mn_3O_4(s)} = 3\mathrm{MnO(s)} + \frac{1}{2}\mathrm{O_2(g)} \quad \Delta G^0 = 232,212 - 117.0T \quad (4)$$

$$\mathrm{Mn_2O_3(s)} = \frac{2}{3}\mathrm{Mn_3O_4(s)} + \frac{1}{6}\mathrm{O_2(g)} \quad \Delta G^0 = 35,062 - 28.07T \quad (5)$$

$$\mathrm{MnO_2(s)} = \mathrm{Mn(s)} + \mathrm{O_2(g)} \quad \Delta G^0 = 518,816 - 181.0T \quad (6)$$

where ΔG^0 is the standard Gibbs free energy; and T is temperature, K.

The decomposition reduction curves of the manganese oxides at different temperatures are calculated by using Eqs. (3)–(6), which are shown in Fig. 3a. It can be seen that the most difficult portion of the manganese oxides reduction process is the reduction of MnO at 1500–1600 °C. If the

Table 2 Composition of molten steel and temperatures during manganese ore direct alloying

No.	Time/min	Composition of molten steel/wt.%						*T*/°C	η_{Mn}
		C	Si	Mn	P	S	Al_s		
1	0	0.04	0.05	0.93	0.008	0.005	0.023	1560	
	1	0.16	0.14	1.12	0.009	0.005	0.045	1552	58.58
	5	0.21	0.21	1.14	0.010	0.005	0.040	1559	65.45
	10	0.22	0.22	1.15	0.010	0.004	0.015	1553	68.44
	15	0.22	0.25	1.17	0.011	0.005	0.012	1556	72.62
	20	0.23	0.33	1.19	0.011	0.004	0.012	1552	79.50
	25	0.23	0.38	1.21	0.011	0.004	0.013	1561	85.48
	30	0.23	0.42	1.22	0.012	0.004	0.021	1553	88.46
2	0	0.06	0.05	1.22	0.020	0.016	0.024	1557	
	1	0.09	0.10	1.39	0.010	0.004	0.065	1553	50.81
	5	0.15	0.17	1.40	0.012	0.004	0.051	1572	54.09
	10	0.17	0.37	1.42	0.012	0.003	0.043	1561	61.86
	15	0.18	0.49	1.43	0.011	0.003	0.037	1540	64.26
	20	0.20	0.55	1.50	0.011	0.003	0.032	1557	83.08
	25	0.23	0.56	1.51	0.012	0.003	0.030	1570	88.16
	30	0.23	0.58	1.53	0.014	0.003	0.028	1567	93.84
3	0	0.05	0.08	1.20	0.009	0.008		1552	
	1	0.10	0.12	1.30	0.009	0.009		1521	30.48
	5	0.12	0.18	1.41	0.009	0.008		1564	65.15
	10	0.14	0.20	1.43	0.010	0.010		1559	69.34
	15	0.18	0.28	1.45	0.008	0.008		1548	77.11
	20	0.20	0.28	1.47	0.008	0.007		1565	82.79
	25	0.22	0.29	1.49	0.009	0.006		1575	86.97
	30	0.22	0.31	1.50	0.010	0.006		1573	90.26
4	0	0.08	0.08	1.11	0.016	0.003		1558	
	1	0.16	0.14	1.22	0.015	0.002		1535	33.17
	5	0.19	0.22	1.33	0.016	0.002		1567	65.75
	10	0.19	0.26	1.37	0.016	0.001		1572	78.90
	15	0.20	0.47	1.38	0.016	0.001		1561	82.49
	20	0.20	0.49	1.39	0.015	0.001		1551	84.88
	25	0.21	0.50	1.39	0.015	0.001		1556	85.18
	30	0.21	0.52	1.40	0.016	0.001		1552	88.16
5	0	0.07	0.05	0.98	0.015	0.005		1555	
	1	0.10	0.19	1.01	0.015	0.007		1538	6.07
	5	0.12	0.21	1.11	0.016	0.003		1553	27.62
	10	0.18	0.37	1.25	0.016	0.005		1567	57.11
	15	0.19	0.39	1.32	0.017	0.004		1554	72.38
	20	0.19	0.38	1.37	0.017	0.006		1567	82.64
	25	0.20	0.44	1.40	0.017	0.006		1576	88.28
	30	0.21	0.45	1.40	0.018	0.006		1567	89.33
6	0	0.07	0.01	1.02	0.014	0.007	0.029	1550	
	1	0.09	0.13	1.10	0.013	0.008	0.032	1570	15.90
	5	0.11	0.15	1.15	0.014	0.005	0.021	1560	26.78
	10	0.16	0.18	1.19	0.015	0.003	0.023	1558	35.36
	15	0.18	0.24	1.24	0.015	0.003	0.017	1554	44.56
	20	0.21	0.34	1.33	0.014	0.002	0.013	1567	63.39
	25	0.22	0.36	1.44	0.014	0.003	0.013	1552	87.66
	30	0.22	0.38	1.46	0.016	0.003	0.011	1554	90.59

Table 3 Composition of slag after direct alloying of manganese ore

No.	Time/min	Composition of slag/wt.%						L_{Mn}
		TFe	CaO	SiO_2	Al_2O_3	MgO	MnO	
1	1	9.89	31.87	7.32	15.23	12.12	10.12	9.04
	5	9.61	32.39	8.19	14.71	14.59	8.97	7.85
	10	9.92	37.71	8.31	12.89	13.30	7.56	6.56
	15	6.36	44.29	8.42	16.18	11.51	6.88	5.90
	20	3.97	49.44	8.48	15.05	11.62	5.47	4.60
	25	4.12	48.98	8.97	15.08	11.87	4.79	3.96
	30	4.44	48.52	9.53	15.51	10.25	4.24	3.47
2	1	5.32	35.50	21.28	15.49	12.03	10.88	7.85
	5	4.02	39.80	22.20	15.60	12.20	7.67	5.49
	10	3.78	40.00	27.85	15.78	12.42	6.49	4.56
	15	3.89	39.78	24.97	14.95	11.62	5.63	3.94
	20	3.28	39.62	25.27	15.01	11.91	5.29	3.54
	25	2.24	39.54	23.80	14.63	12.74	4.35	2.88
	30	2.56	39.73	22.65	14.97	12.68	3.08	2.01
3	1	6.25	32.60	25.80	1.49	10.30	9.88	7.62
	5	4.02	38.80	24.20	1.60	11.20	8.17	5.78
	10	3.78	41.20	27.50	1.78	11.42	7.69	5.38
	15	2.39	40.78	25.70	1.95	11.62	7.38	5.07
	20	2.28	40.62	26.30	1.01	12.91	6.29	4.27
	25	2.24	40.54	24.80	1.63	12.74	5.35	3.60
	30	2.56	40.73	23.50	1.97	12.68	5.08	3.40
4	1	4.49	40.67	22.90	2.97	10.10	9.73	7.98
	5	5.83	40.58	22.91	2.97	11.10	7.43	5.59
	10	4.83	41.53	23.94	3.56	12.20	6.75	4.92
	15	6.89	40.68	22.90	2.97	13.10	4.73	3.42
	20	5.29	49.61	21.38	3.98	13.70	4.13	2.97
	25	4.89	40.69	22.92	2.97	13.10	3.73	2.67
	30	3.89	40.65	22.91	2.97	14.10	2.73	1.95
5	1	6.14	32.20	30.91	3.66	10.34	10.95	10.90
	5	5.79	22.91	33.95	3.51	14.13	9.54	8.61
	10	2.14	32.80	31.91	3.56	11.34	8.95	7.16
	15	1.28	35.34	38.85	4.44	11.07	8.41	6.36
	20	3.38	36.48	29.77	3.84	13.74	6.96	5.07
	25	1.20	38.76	31.65	3.75	13.87	5.83	4.17
	30	1.15	37.97	30.98	3.92	15.93	4.81	3.43
6	1	5.88	31.18	12.06	17.03	11.24	10.99	10.00
	5	2.89	30.49	13.89	20.87	12.90	9.78	8.51
	10	2.74	31.48	15.33	22.06	12.30	9.27	7.78
	15	3.84	31.30	17.33	21.68	13.10	8.53	6.91
	20	5.88	30.81	18.06	21.03	13.40	6.99	5.28
	25	6.35	31.15	15.61	24.57	13.97	5.77	4.00
	30	2.01	35.89	14.83	25.52	13.99	3.33	2.28

reduction of MnO in the manganese ore can be achieved in this temperature range, the process would be successful.

In this experiment, carbon powder, aluminum and ferrosilicon powder were used as reducing agents and the following reactions occurred during the steelmaking process [24].

$$C(s) + \frac{1}{2}O_2(g) = CO(g) \quad \Delta G^0 = -114,400 - 85.77T \tag{7}$$

$$Si(s) + O_2(g) = SiO_2(s) \quad \Delta G^0 = -904,760 - 173.38T \tag{8}$$

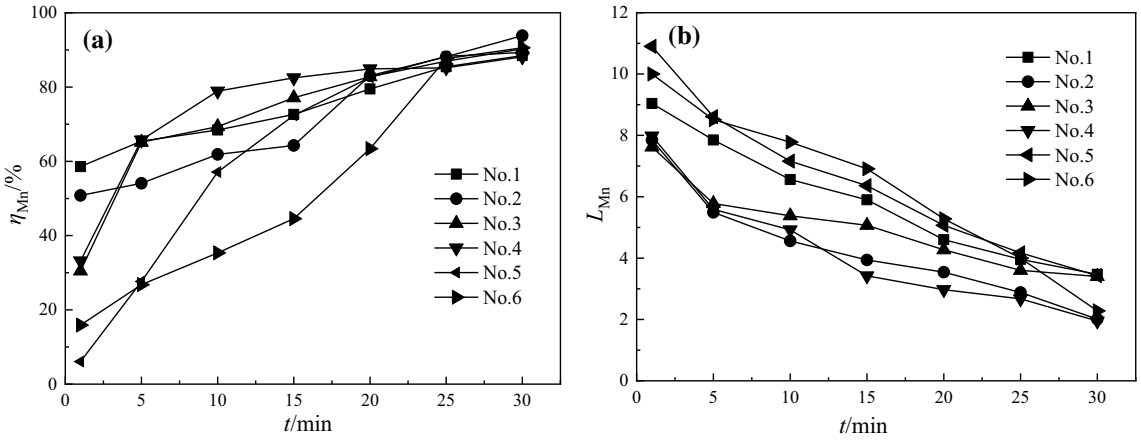

Fig. 2 Manganese yield (**a**) and manganese distribution ratio between slag and steel (**b**) at different refining time *t*

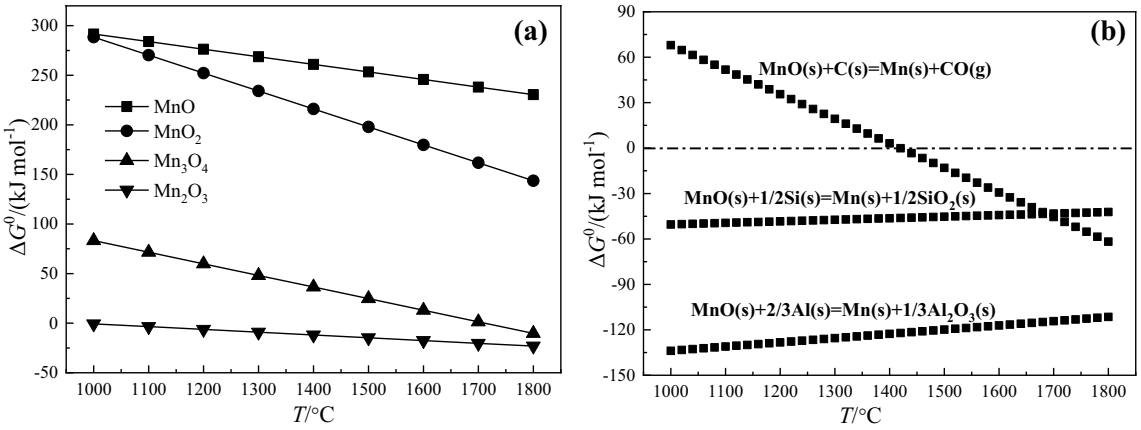

Fig. 3 Decomposition of manganese oxide (**a**) and reduction curve of manganese oxide by carbon, silicon and aluminum (**b**)

$$2\mathrm{Al(s)} + \frac{3}{2}\mathrm{O_2(g)} = \mathrm{Al_2O_3(s)} \quad \Delta G^0 = -1,675,100 - 313.20T. \tag{9}$$

According to Eqs. (3) and (7)–(9), the following equations can be obtained:

$$\mathrm{C(s) + MnO(s) = Mn(s) + CO(g)} \quad \Delta G^0 = 274,460 - 162.19T \tag{10}$$

$$\frac{1}{2}\mathrm{Si(s) + MnO(s) = Mn(s) + \frac{1}{2}SiO_2(s)} \quad \Delta G^0 = -63,520 + 10.27T \tag{11}$$

$$\frac{2}{3}\mathrm{Al(s) + MnO(s) = Mn(s) + \frac{1}{3}Al_2O_3(s)} \quad \Delta G^0 = -169,506.67 + 27.98T. \tag{12}$$

The Gibbs free energy change of the three different reduction reactions can be obtained by using Eqs. (10)–(12) and is shown in Fig. 3b. It can be seen that the three reactions occurred in the refining temperature range of 1540–1600 °C.

Figure 3b shows that the Gibbs free energy of reaction between aluminum or silicon and MnO is lower than that of carbon and MnO within 1700 °C; thus, the reactions between aluminum or silicon and MnO are stronger than that between carbon and MnO. It can be seen from Eqs. (10)–(12) that the main factors affecting the manganese ore reduction are the temperature and the activities of various components such as aluminum, silicon and carbon.

Figure 4 shows the effect of the compositions of molten steel and slag and the temperature on the manganese yield, which is obtained from Tables 1 and 2. For wire feeding process, the most important factor affecting the manganese yield is the carbon content in molten steel, followed by iron oxide content in slag, silicon content in molten steel, molten steel temperature and slag basicity. The content of acid-soluble aluminum in molten steel has no significant effect on the manganese yield. With increasing the carbon and silicon contents in molten steel and basicity of slag, as well as decreasing the temperature of molten steel and the

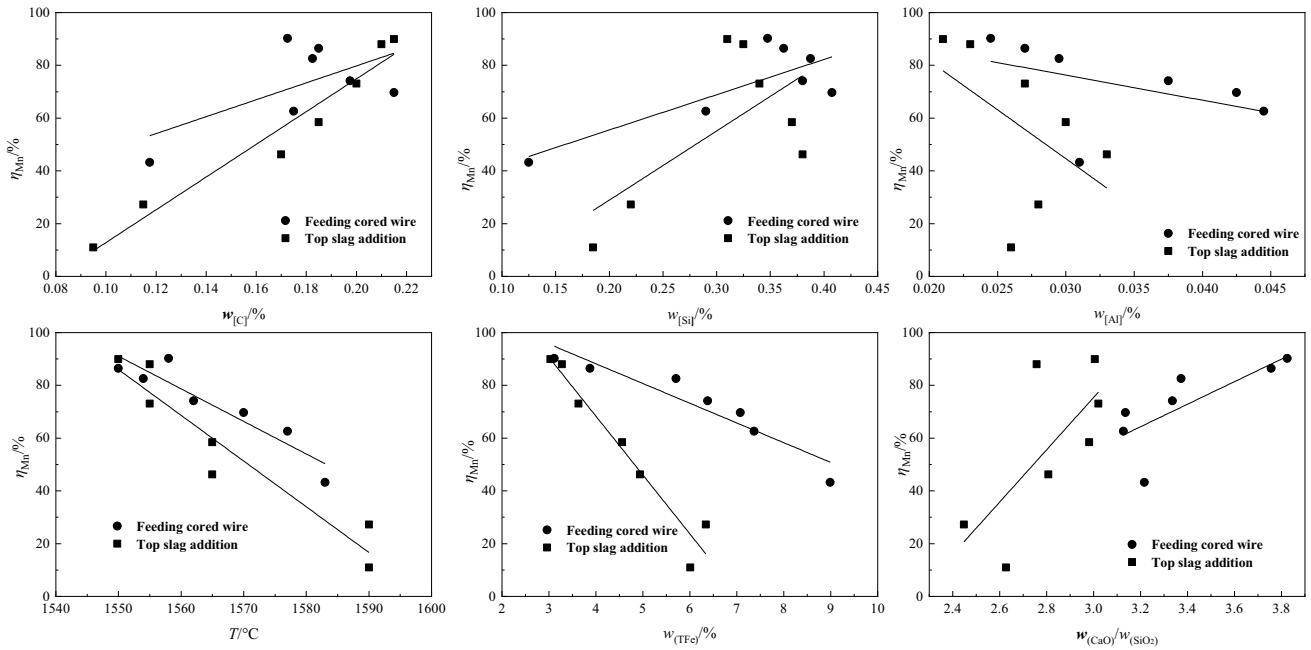

Fig. 4 Effect of compositions of molten steel and slag and temperature on manganese yield

content of iron oxide, the manganese yield increased in different degrees.

For the top-slag adding process, the most important factor affecting the manganese yield is the silicon content in molten steel, followed by carbon content in molten steel, acid-soluble aluminum content in molten steel, molten steel temperature, slag basicity and iron oxide content in slag.

Therefore, increasing the silicon and carbon contents in molten steel and the basicity of slag or reducing the acid-soluble aluminum content in molten steel, the temperature of molten steel and the content of iron oxide in slag is beneficial to increasing the manganese yield.

4.2 Analysis of influencing factors on manganese distribution ratio in molten steel and slag

During the reduction process of the manganese ore, the following reactions occur [25]:

$$(\mathrm{MnO}) + [\mathrm{C}] = [\mathrm{Mn}] + \mathrm{CO(g)} \quad \Delta G^0 = 259,826 - 129.06T \tag{13}$$

$$\lg \frac{w_{(\mathrm{MnO})}}{w_{[\mathrm{Mn}]}} = \frac{13,570}{T} - \lg \frac{\gamma_{\mathrm{MnO}}}{f_{\mathrm{Mn}}} - \lg f_{\mathrm{C}} - \lg w_{[\mathrm{C}]} - 6.74 \tag{14}$$

where γ_{MnO} is the activity coefficient of MnO in slag; f_{Mn} is the manganese activity coefficient in metal solution; and f_{C} is the carbon activity coefficient in metal solution.

Equation (14) shows the influencing laws on L_{Mn}. An increase in the carbon content of the molten steel results in a decrease in the manganese distribution ratio between slag and steel; as the temperature of the molten steel increases, the manganese distribution ratio between slag and steel decreases.

$$3(\mathrm{MnO}) + [\mathrm{Si}] = (\mathrm{MnO} \cdot \mathrm{SiO_2}) + 2[\mathrm{Mn}] \quad \Delta G^0 = -116,743 - 2.049T \tag{15}$$

$$\lg \frac{w_{(\mathrm{MnO})}^{3/2}}{w_{[\mathrm{Mn}]}} = -\frac{3048.6}{T} - \lg \frac{\gamma_{\mathrm{MnO}}^{3/2}}{f_{\mathrm{Mn}}} - \frac{1}{2}\lg f_{\mathrm{Si}} - \frac{1}{2}\lg w_{[\mathrm{Si}]} + \frac{1}{2}\lg a_{\mathrm{MnO\cdot SiO_2}} - 0.053 \tag{16}$$

where f_{Si} is the silicon activity coefficient in metal solution and $a_{\mathrm{MnO\cdot SiO_2}}$ is the activity of $\mathrm{MnO\cdot SiO_2}$ in slag.

Equation (16) shows that an increase in the silicon content of molten steel results in a decrease in the manganese distribution ratio between slag and steel, and a decrease in the temperature of molten steel leads to a decrease in the manganese distribution ratio between slag and steel.

$$4(\mathrm{MnO}) + 2[\mathrm{Al}] = \mathrm{MnO} \cdot \mathrm{Al_2O_3(s)} + 3[\mathrm{Mn}] \quad \Delta G^0 = -538,813 - 67.3T \tag{17}$$

$$\lg \frac{w_{(\mathrm{MnO})}^{4/3}}{w_{[\mathrm{Mn}]}} = -\frac{9380.29}{T} - \lg \frac{\gamma_{\mathrm{MnO}}^{4/3}}{f_{\mathrm{Mn}}} + \frac{1}{3}\lg a_{\mathrm{MnO\cdot Al_2O_3}} - \frac{2}{3}\lg f_{[\mathrm{Al}]} - \frac{2}{3}\lg w_{[\mathrm{Al}]} + 1.17 \tag{18}$$

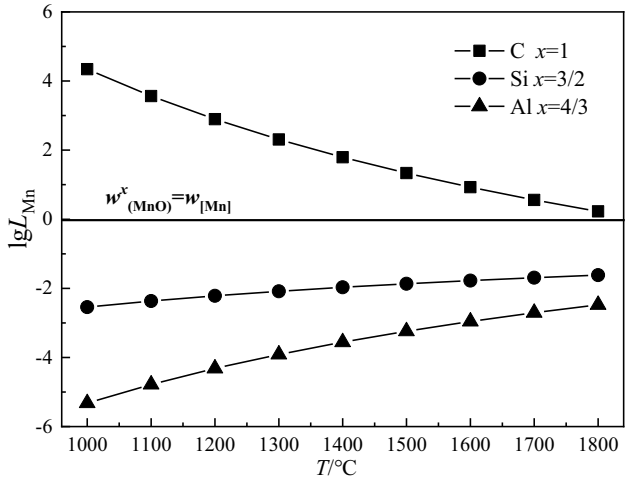

Fig. 5 Relationship between manganese distribution ratio and temperature with different reducing agents

where f_{Al} is the aluminum activity coefficient in metal solution and $a_{MnO\cdot Al_2O_3}$ is the activity of $MnO\cdot Al_2O_3$ in slag.

Equation (18) shows that an increase in the acid-soluble aluminum content of molten steel causes a decrease in the manganese distribution ratio between slag and steel, and a decrease in the temperature of the molten steel also decreases the manganese distribution ratio between slag and steel.

Thus, in order to reduce the manganese content in the slag, the content of the reducing agent (carbon, silicon and aluminum) should be increased and the temperature has to be controlled.

Figure 5 shows the relationship of the manganese distribution ratio between slag and metal to the temperature based on Eqs. (14), (16) and (18) by using different reducing agents. The activity coefficients of the elements are obtained from Ref. [9].

The activity coefficients of the MnO in the slag are obtained from Ref. [26] and the following equation:

$$\lg \gamma_{MnO} = 0.0415(w_{(CaO)} + 0.45w_{(SiO_2)} + 0.60w_{(MgO)} + 0.66w_{(Fe_tO)} + 0.45w_{(MnO)} + 0.95w_{(P_2O_5)}) + \frac{803}{T} - 3.075. \quad (19)$$

Figure 5 shows that when the aluminum and ferrosilicon are used as deoxidizer, the manganese distribution ratio between slag and steel is proportional to the temperature.

Figure 6 depicts the effect of the compositions of molten steel and slag as well as the temperature on the manganese distribution ratio between slag and metal. For wire feeding process, the largest factor affecting the manganese distribution ratio between slag and metal is the content of iron oxide in slag, followed by the content of acid-soluble aluminum in molten steel, carbon content in molten steel, temperature of molten steel, silicon content in molten steel and basicity of slag.

For the process of top-slag adding, the biggest factor affecting manganese distribution ratio between slag and steel is iron oxide content in slag, followed by carbon content in molten steel, acid-soluble aluminum content in molten steel, silicon content in molten steel, molten steel temperature and slag basicity.

For the two processes, increasing the silicon content, carbon content and basicity of slag or reducing the acid-soluble aluminum content of molten steel, the temperature of molten steel and the content of iron oxide in slag, the manganese distribution ratio between slag and steel increased in different degrees.

It can also be observed from Fig. 6 that the manganese distribution ratio between slag and steel increases with increasing the temperatures of molten steel. The results show that aluminum and silicon are the most effective deoxidation agents for the two processes.

4.3 Mass transfer rate of manganese in molten steel and slag

The influence of the two processes on the manganese transfer in the slag and molten steel is discussed by kinetics.

$$(MnO) = [Mn] + [O] \quad (20)$$

The manganese ore reduction is related to the manganese transfer at the slag and molten steel interface, as shown in Eq. (20). It is assumed that the mass transfer of [Mn] and [O] in the molten steel is the limiting factor; the reaction rate is expressed as follows:

$$\frac{dw_{[Mn]}}{dt} = \frac{A}{V}\beta_{Mn}(w_{[Mn]} - w^*_{[Mn]}) \quad (21)$$

$$\frac{dw_{[Mn]}}{(w_{[Mn]} - w^*_{[Mn]})} = \frac{A}{V}\beta_{Mn}dt \quad (22)$$

$$\lg\left(\frac{w_{[Mn],\,t} - w^*_{[Mn]}}{w_{[Mn],\,i} - w^*_{[Mn]}}\right) = \frac{A}{V}\beta_{Mn}t \quad (23)$$

where A is the bath surface area, m^2; V is the volume of the slag, m^3; $w_{[Mn],\,t}$ is the weight percentage of the manganese in molten steel at time t, %; $w^*_{[Mn]}$ is the weight percentage of the manganese in the molten steel at manganese equilibrium, %; and β_{Mn} is the mass transfer coefficient of the manganese in the molten steel, m/s.

Figure 7a shows the changes in the manganese content at different time. The slope values corresponding to the furnace

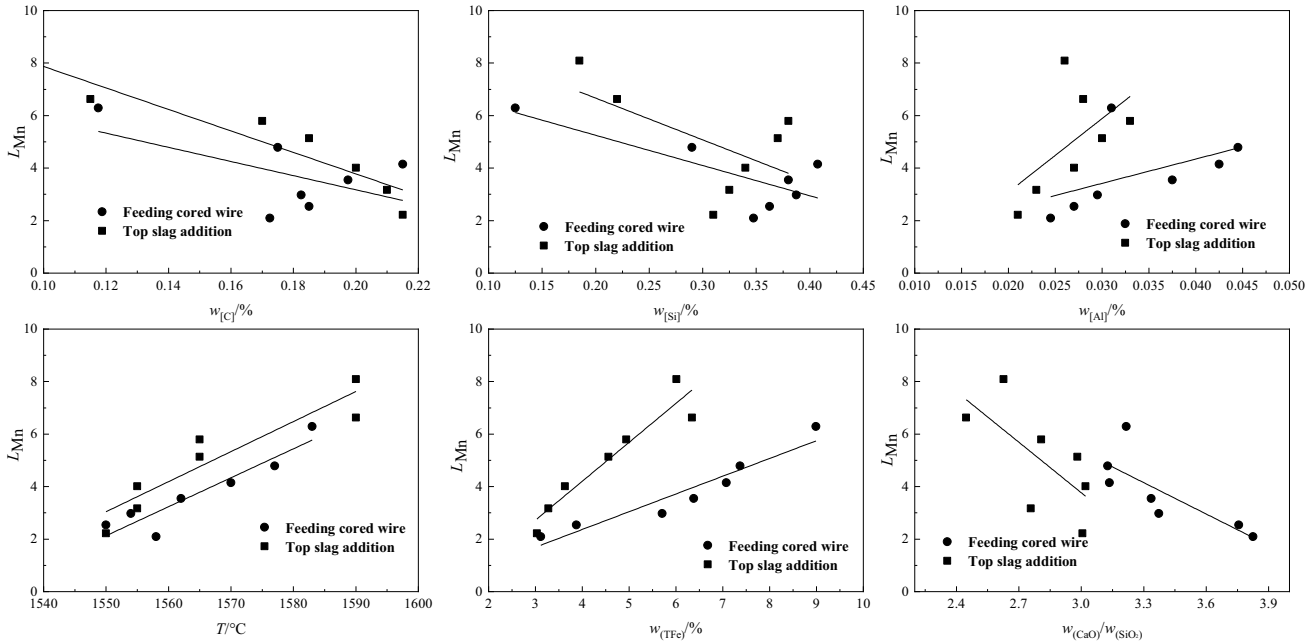

Fig. 6 Effect of compositions of molten steel and slag and temperature on manganese distribution ratio between slag and metal

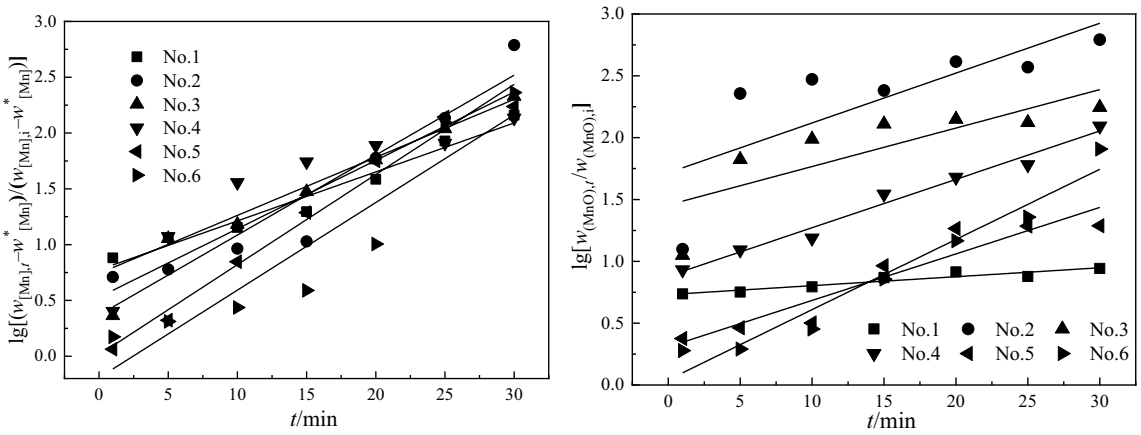

Fig. 7 Changes in manganese content in molten steel and manganese oxide content in slag at different blowing time. **a** Mass transfer in molten steel; **b** mass transfer in slag. $w_{(MnO),t}$ Mass fraction of MnO in slag at time t; $w_{(MnO),i}$ mass fraction of MnO in initial slag

tests Nos. 1–6 are 0.044, 0.072, 0.061, 0.052, 0.081 and 0.079 L/min, respectively.

When the density of the slag is 2.9 kg/m^3, the molten bath area is 0.11 m^3, the bath diameter is 0.38 m, the molten steel mass is 200 kg, the slag mass range is 3.9–5.5 kg, and the manganese ore mass is 1.4 kg. By using Eq. (23) and these parameters, the mass transfer coefficients corresponding to the six furnace tests can be calculated and the β_{Mn} values are 0.0091, 0.0180, 0.0140, 0.0100, 0.0200 and 0.0220 m/s, respectively.

The mass transfer rate v of MnO in the slag is expressed as follows:

$$v = -\frac{\mathrm{d}w_{(\mathrm{MnO})}}{\mathrm{d}t} = \beta_{\mathrm{MnO}}(w_{(\mathrm{MnO})} - w^*_{(\mathrm{MnO})}) \cdot \frac{A}{V} \tag{24}$$

$$V = \frac{m_{\mathrm{slag}}}{\rho_{\mathrm{slag}}} \tag{25}$$

where $w^*_{(\mathrm{MnO})}$ is the MnO concentration on the slag surface at manganese equilibrium, %; m_{slag} is the mass of the slag, kg; ρ_{slag} is the density of the slag; and β_{MnO} is the mass transfer coefficient of the slag layer, m/s. The value of $w^*_{(\mathrm{MnO})}$ is zero.

Equations (24) and (25) can be further simplified into:

$$-\frac{\mathrm{d}w_{(\mathrm{MnO})}}{\mathrm{d}t}=\frac{A\beta_{\mathrm{MnO}}\rho_{\mathrm{slag}}}{m_{\mathrm{slag}}}w_{(\mathrm{MnO})}, \tag{26}$$

while the integral is

$$-\lg\frac{w_{(\mathrm{MnO}),t}}{w_{(\mathrm{MnO}),0}}=\frac{A\beta_{\mathrm{MnO}}\rho_{\mathrm{slag}}}{m_{\mathrm{slag}}}t. \tag{27}$$

The change in the manganese content in the slag over time is displayed in Fig. 7b. The slope values corresponding to the furnace tests Nos. 1–6 are 0.007, 0.040, 0.031, 0.039, 0.038 and 0.057 L/min, respectively.

By using Eq. (27) and the above parameters, the mass transfer coefficients of MnO in slag corresponding to the six tests are 0.0012, 0.0078, 0.0054, 0.0060, 0.0074 and 0.0120 m/s, respectively.

The comparison of the mass transfer coefficients of the manganese in the molten steel and slag is shown in Fig. 8. For the range of 0–30 min, the mass transfer velocity of the manganese is greater in the molten steel than in the slag, and the mass transfer of the manganese in the slag is the limiting factor.

4.4 Changes in slag composition during manganese ore reduction

Figure 9 shows positions in the phase diagram of the slag composition for the wire feeding and top-slag adding processes, in which the slag of wire feeding process obtained is closer to the area of high melting point. The melting point of slag is slightly higher for the top-slag adding process than for the wire feeding process. Figures 10 and 11 show the result of the TG (thermogravimetric analysis) and DSC (differential scanning calorimetry), which were measured using a thermogravimetric analyzer with wire feeding and top-slag adding processes at 15, 25 and 30 min, and Table 4 shows the melting point measured using a thermogravimetric analyzer. Based on Figs. 9–11 and Table 4, it can be seen that the melting point calculated from the phase diagram is higher than the measured value, but the trend is identical.

Figure 12 shows the composition of the slag phase for the top-slag adding process. During the slag phase (15 min), olivine composed of CaO, SiO_2 and MnO is present, the reduction reaction of the slag is incomplete, and the refining slag has not formed. At 25 min, the refining slag has formed and the slag begins to nucleate and grow. The refining slag composed of CaO, SiO_2 and MgO is formed at 30 min.

Figure 13 shows the composition of the slag phase during the process of adding the manganese ore cored wire. The slag phase is characterized by the formation of the refining

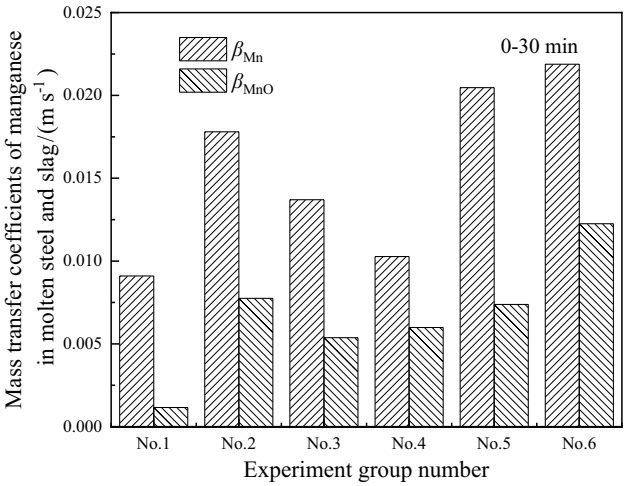

Fig. 8 Comparison of mass transfer coefficients of manganese in slag and molten steel at 0–30 min

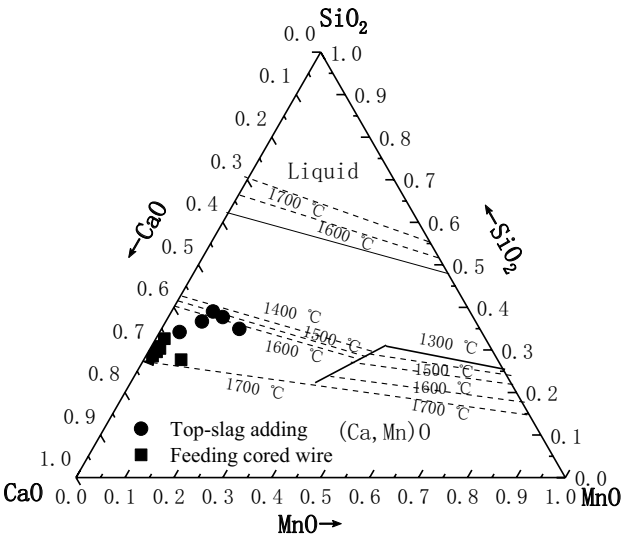

Fig. 9 Slag composition during manganese reduction

slag composed of CaO and SiO_2 at 15 min. At 25 min, the refining slag has formed and begins to nucleate and grow. The CaO and SiO_2 minerals contain P_2O_5. The refining slag composed of CaO, SiO_2 and Al_2O_3 is formed at 30 min and is well developed.

The compositions of the slag for the wire feeding and the top-slag adding processes detected by energy spectrum are shown in Table 4. In the top-slag adding process, the manganese oxide of slag is significantly more than that of the wire feeding process. Compared with the wire feeding process, when adding the manganese ore by top slag, the acidic component of the slag, i.e., manganese oxide, is higher, and

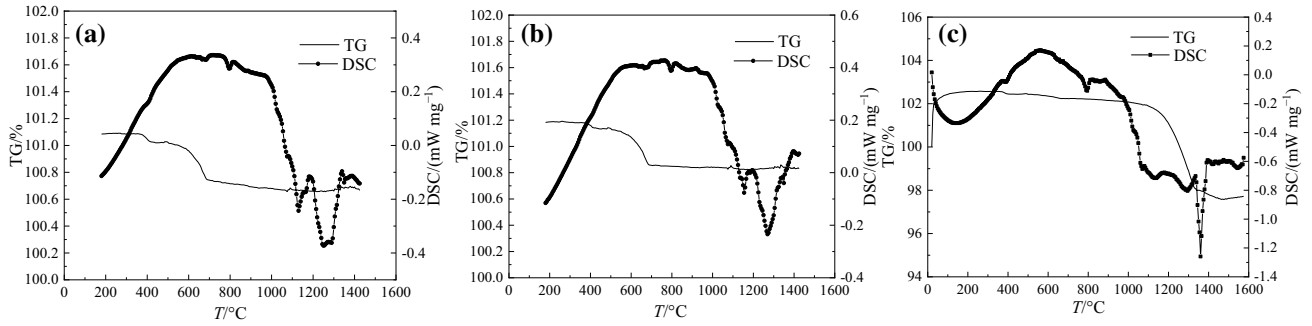

Fig. 10 TG and DSC during top-slag adding process at 15 min (**a**), 25 min (**b**) and 30 min (**c**)

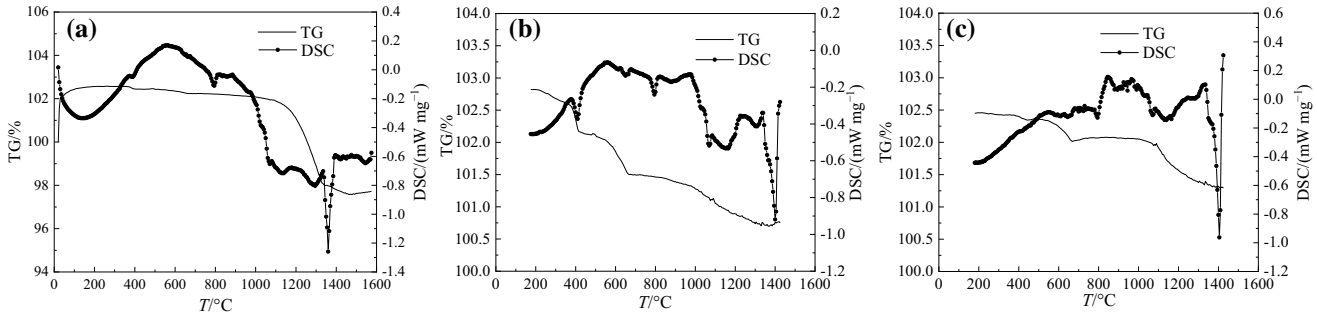

Fig. 11 TG and DSC during wire feeding process at 15 min (**a**), 25 min (**b**) and 30 min (**c**)

Table 4 Composition and melting point of slag for wire feeding and top-slag adding process detected by energy spectrum

Time	Top slag (Fig. 12)		Wire feeding (Fig. 13)	
	Composition	Melting point/°C	Composition	Melting point/°C
15 min	1-CaO, SiO_2, MnO; 2-CaO, SiO_2, MnO	1205	2-CaO, SiO_2, MgO, Al_2O_3	1359
25 min	1-Fe, Mn alloy; 2- CaO, SiO_2, FeO, MnO	1226	3-FeO, CaO, MgO; 4-CaO, SiO_2, P_2O_5	1345
End	1-CaO, SiO_2, MnO; 2-CaO, SiO_2, MgO	1360	5-MgO, Al_2O_3; 6-CaO, SiO_2, Al_2O_3	1399

the slag basicity is low, so that the melting point of the slag is lower. This should prove that the top-slag adding process has a low reaction rate and insufficient reaction.

5 Conclusions

1. The manganese yield is higher than 90% when the wire feeding method is used. The manganese yield is 43.26% after 1 min. In contrast, the manganese yield for the top-slag adding process is only 10.98% for the same duration.
2. The manganese distribution ratio between slag and steel can be decreased by either increasing the carbon and silicon contents in the molten steel and the slag basicity or by reducing the acid-soluble aluminum content in the molten steel and the TFe content in the slag.
3. The mass transfer rate of the manganese is greater in the molten steel than in the slag, and the limiting factor is the mass transfer of the manganese in the slag in the period of 0–30 min.
4. The slag composition area is closer to the area of high melting point when the wire feeding method is used.
5. The manganese ore wire feeding method forms the refining slag composed of CaO and SiO_2 at 15 min; after 25–30 min, the refining slag with high basicity is formed and consists of CaO, SiO_2 and Al_2O_3.

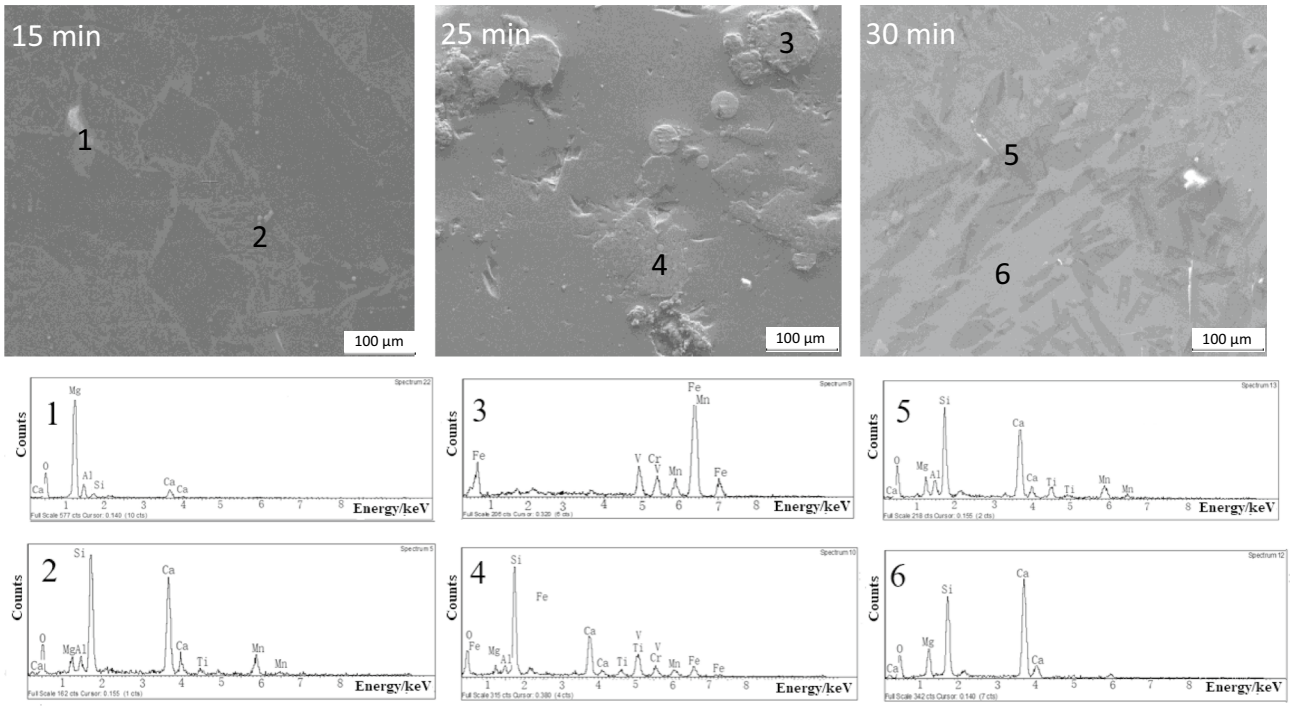

Fig. 12 Composition of slag phase for top-slag adding process

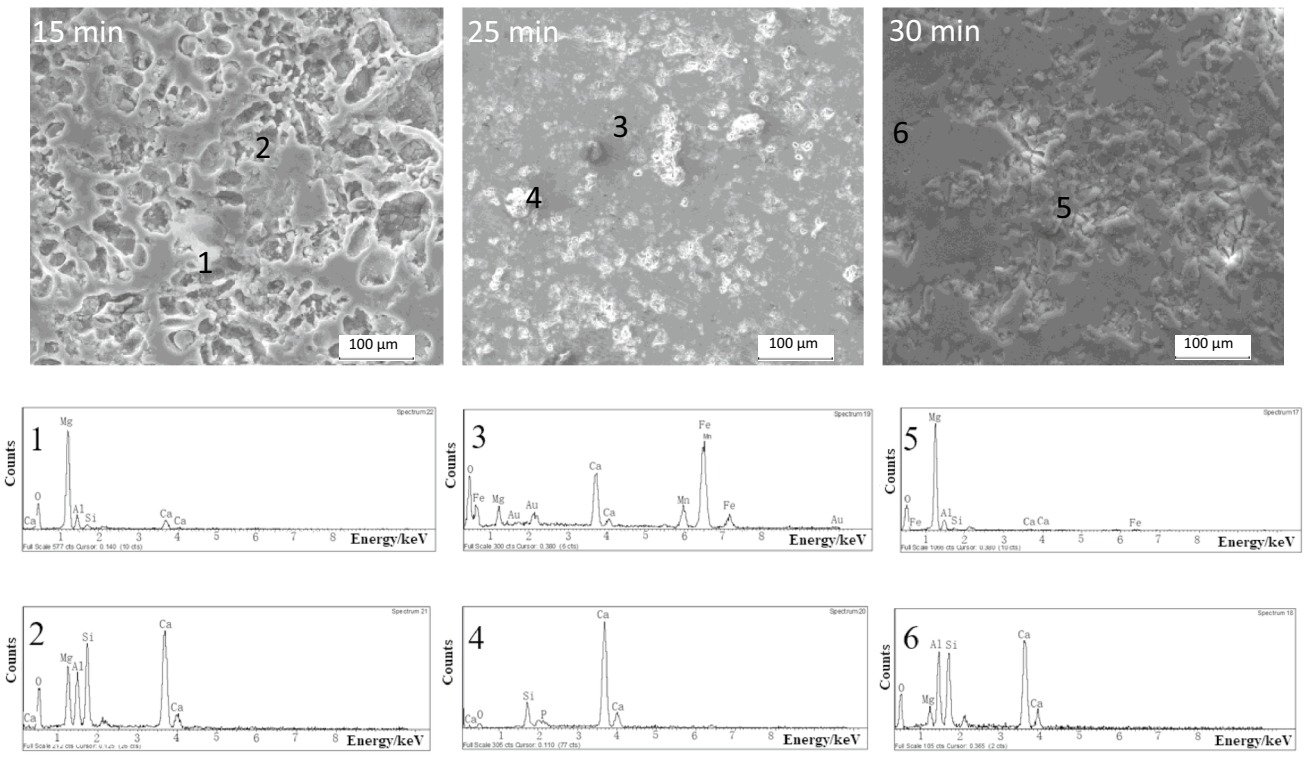

Fig. 13 Composition of slag phase for manganese ore cored wire feeding method

Acknowledgements This research has been financially supported by the National Key R&D Program (2017YFB0304000) and the Beijing Natural Science Foundation (2172057) in China, the State Key Laboratory of Refractories and Metallurgy Foundation (G201804) and the National Natural Science Foundation of China (51704080, 51874102).

References

[1] W. Wu, S.F. Dai, P. Wang, D. Ma, B. Ni, Ironmak. Steelmak. 46 (2019) 469−476.
[2] W. Wu, S.F. Dai, Y. Liu, J. Iron Steel Res. Int. 24 (2017) 908–915.
[3] W. Wu, J.J. Gao, J.Q. Zeng, Y.H. Qi, J.C. Wang, X.D. Zhang, J. Iron Steel Res. Int. 23 (2016) 210–219.
[4] L.N. Guo, J. Chen, M. Zhang, M. Liang, J. Iron Steel Res. Int. 19 (2012) No. 5, 1–8.
[5] J. Chen, P.F. Tian, X.A. Song, N. Li, J.X. Zhou, J. Iron Steel Res. Int. 17 (2010) No. 3, 13–20.
[6] S.F. Dai , W. Wu, D. Ma, X.D. Zhang, P. Wang, Iron and Steel 52 (2017) No. 8, 35–42.
[7] T. Shimoo, S. Ando, H. Kimura, J. Jpn. Inst. Met. 48 (1984) 285–292.
[8] T. Shimoo, S. Ando, H. Kimura, J. Jpn. Inst. Met. 48 (1984) 922–929.
[9] K.D. Xu, G.C. Jiang, W.Z. Ding, L.P. Gu, S.Q. Guo, B.X. Zhao, ISIJ Int. 33 (1993) 104–108.
[10] M. Ashizuka, A. Moribe, K. Sawamura, Tetsu-to-Hagane 61 (1975) 36–45.
[11] D.Y. Kim, S.M. Jung, ISIJ Int. 56 (2016) 71–77.
[12] N. Shinozaki, K. Ishido, K. Mori, Y. Kawai, Tetsu-to-Hagane 70 (1984) 73–80.
[13] R. Kononov, O. Ostrovski, S. Ganguly, Metall. Mater. Trans. B 39 (2008) 662–668.
[14] N. Anacleto, O. Ostrovski, S. Ganguly, ISIJ Int. 44 (2004) 1615–1622.
[15] O.I. Ostrovski, T.J.M. Webb, ISIJ Int. 35 (1995) 1331–1339.
[16] S.F. Dai, W. Wu, X.D. Zhang, P. Wang, China Metallurgy 27 (2017) No. 1, 12–18.
[17] W. Wu, P. Wang, L. Lin, S.F. Dai, High Temperature Materials and Processes 37 (2018) 741–747.
[18] C.F. Zhang, J.B. Chang, S.W. Li, Z.J. Han, D.G. Ma, S.X. Liu, Y.B. Xiang, Steelmaking 29 (2013) No. 6, 12–14.
[19] C.F. Lv, D.L. Shang, Q. Sun, L. Kang, Z.Y. Qi, Steelmaking 31 (2015) No. 1, 40–43.
[20] T. Takaoka, I. Sumi, Y. Kikuchi, Y. Kawai, ISIJ Int. 33 (1993) 98–103.
[21] J. Safarian, Ø. Grong, L. Kolbeinsen, S.E. Olsen, ISIJ Int. 46 (2006) 1120–1129.
[22] T. Matsuo, S. Fukagawa, T. Ikeda, Tetsu-to-Hagane 76 (1990) 1831–1838.
[23] O.A. El Hady, A.E. Amer, I.S. El Mahallawi, Y.S. Shash, Mater. Sci. Forum 561–565 (2007) 85–89.
[24] S.M. Jung, C.H. Rhee, D.J. Min, ISIJ Int. 42 (2002) 63–70.
[25] E.T. Turkdogan, Fundamentals of steelmaking, The Institute of Materials Publishers, London, UK, 1996.
[26] A. Sobandi, H.G. Katayama, T. Momono, ISIJ Int. 38 (1998) 953–958.